Publications

5-28-2004

Re-defining the Empirical ZZ Ceti Instability Strip

Anjum S. Mukadam
University of Texas

Ted von Hippel
University of Texas, vonhippt@erau.edu

D. E. Winget,
University of Texas

M. H. Montgomery
University of Texas

Scholarly Commons Citation

Re-defining the Empirical ZZ Ceti Instability Strip

Anjum S. Mukadam, D. E. Winget, Ted von Hippel, M. H. Montgomery

Department of Astronomy, University of Texas at Austin, Austin, TX -78712, U.S.A.;
anjum@astro.as.utexas.edu

McDonald Observatory, Fort Davis, TX 79734, U.S.A.

S. O. Kepler, A. F. M. Costa

Instituto de Física, Universidade Federal do Rio Grande do Sul, 91501-970 Porto Alegre,
RS - Brazil.

ABSTRACT

We use the new ZZ Ceti stars (hydrogen atmosphere white dwarf variables; DAVs) discovered within the Sloan Digital Sky Survey (Mukadam et al. 2004) to re-define the empirical ZZ Ceti instability strip. This is the first time since the discovery of white dwarf variables in 1968 that we have a homogeneous set of spectra acquired using the same instrument on the same telescope, and with consistent data reductions, for a statistically significant sample of ZZ Ceti stars. The homogeneity of the spectra reduces the scatter in the spectroscopic temperatures and we find a narrow instability strip of width $\sim 950\,\mathrm{K}$, from 10850–11800 K. We question the purity of the DAV instability strip as we find several non-variables within. We present our best fit for the red edge and our constraint for the blue edge of the instability strip, determined using a statistical approach.

Subject headings: stars:oscillations–stars: variables: other–white dwarfs

1. Introduction

Global pulsations in white dwarf stars provide the only current systematic way to study their interiors. Hydrogen atmosphere white dwarfs (DAs) exhibit nonradial g-mode pulsations, and are known as DA Variables (DAVs) or ZZ Ceti stars. Bergeron et al. (1995, 2004) and Koester & Allard (2000) find these pulsators confined in the range $11\,000\,\mathrm{K}$ and $12\,500\,\mathrm{K}$ for $\log g \approx 8$.

During the course of a 15 month long search, Mukadam et al. (2004, hereafter Paper-I) discovered 35 new ZZ Ceti stars within the Sloan Digital Sky Survey (SDSS). This is

the first time in the history of white dwarf asteroseismology that we have a statistically significant homogeneous set of ZZ Ceti spectra, acquired entirely with the same detection system, namely the SDSS spectrograph on the 2.5 m telescope at Apache Point Observatory. All the spectra have been reduced and analyzed consistently using the same set of model atmospheres and fitting algorithms, including the observed photometric colors (see Kleinman et al. 2004). This homogeneity should reduce the relative scatter of the variables in the T_{eff}– log g plane, and possibly allow us to see emerging new features. The sample size of known DAVs is now almost twice as large since the last characterization of the instability strip by Bergeron et al. (2004). However, we will not include the previously known DAVs in our analysis with the exception of G 238-53, as these pulsators do not have SDSS spectra and will only serve to reduce the homogeneity of our sample.

We list the T_{eff} and log g values of all the variables and non-variables we discovered within the SDSS data in Paper-I, along with their internal uncertainties. Note that we will not be considering WD2350−0054 in this paper as it may be a unique pulsator; it shows pulsation periods and pulse shapes characteristic of the hot DAV stars, while the SDSS temperature determination places it below the cool edge of the instability strip. We focus on the general trends of the majority of the DAVs, and hence a discussion of WD2350−0054 is postponed to a future date. We will not be including WD1443−0054 either, as its temperature and log g determinations are unreliable due to a missing portion in its SDSS spectrum. We will be including G 238-53, the only previously known ZZ Ceti star with a published SDSS spectrum.

2. Empirical instability strip

We show the empirical SDSS instability strip in Figure 1, as determined by 30 new ZZ Ceti stars and G 238-53. We plot histograms of the observed variables as a function of temperature and log g, and weighted histograms (see section 2.2) for the non-variables (Not Observed to Vary; NOVs). Figure 1 has two striking features: a narrow strip of width 950 K and non-variable DA white dwarfs within the instability strip.

Pulsations are believed to be an evolutionary effect in otherwise normal white dwarfs (Robinson 1979; Fontaine et al. 1985; Fontaine et al. 2003; Bergeron et al. 2004). Non-variables in the middle of the strip question this semi-empirical premise, even if we use the uncertainties in temperature to justify the non-variables close to the edges.

We also note that the DAV distribution appears to be non-uniform across the strip. The features of this plot are influenced by various factors such as biases in candidate selection,

non-uniform detection efficiency in the T_{eff}–log g plane, and uncertainties as well as systematic effects in spectroscopic temperature and log g determinations. We address these issues and their effects on the DAV distribution in the next few sub-sections.

2.1. Biases in Candidate Selection

We selected SDSS DAV candidates for high-speed photometry from those spectroscopically identified DA white dwarfs that lie in the temperature range 11000–12500 K. These temperature fits are derived by our SDSS collaborators using the spectral fitting technique outlined in Kleinman et al. (2004). Paper-I gives a discussion of other candidate selection methods used in our search for ZZ Ceti stars prior to the spectral fitting technique.

Our various science goals lead to some biases in selecting DAV candidates for observation. The hot DAV (hDAV) stars exhibit extreme amplitude and frequency stability (e.g. Kepler et al. 2000a; Mukadam et al. 2003). We plan to search for reflex motion caused by orbiting planets around such stable pulsators (e.g. Kepler et al. 1991; Mukadam, Winget, & Kepler 2001; Winget et al. 2003). These stable clocks drift at their cooling rate; measuring the drift rate in the absence of orbital companions allows us to calibrate our evolutionary models. These models are useful in determining ages of the Galactic disk and halo using white dwarfs as chronometers (e.g. Winget et al. 1987; Hansen et al. 2002). Therefore, we preferentially choose to observe hDAV candidates in the range 11700–12300 K to increase the sample of known stable pulsators with both the above objectives in mind. This bias is partially compensated for, as hDAVs are harder to find (see section 2.2).

We also preferentially observe DAV candidates of extreme masses. Low mass (log $g \leq$ 7.6) DAVs could well be helium core white dwarfs; pulsating He core white dwarfs should allow us to probe their equation of state. High mass (log $g \geq$ 8.5) DAVs are potentially crystallized (Winget et al. 1997; Montgomery & Winget 1999), providing a test of the theory of crystallization in stellar plasma. Metcalfe, Montgomery, & Kanaan (2004) present strong evidence that the massive DAV, BPM 37093, is 90% crystallized.

The distribution of *chosen* DAV candidates also depends on the distribution of *available* DAV candidates. We have an additional bias due to the SDSS criteria in choosing candidates for spectroscopy. But a histogram of the available DAV candidates is consistent with a random distribution and does not reflect any systematic effects.

The non-uniform nature of the DAV distribution does not appear to be a candidate selection effect. However, we are in the domain of small number statistics since we observed only four DAV candidates in the range 11350–11500 K. Of these, two are massive and conse-

quently expected to be low amplitude pulsators (see section 2.2), making detection difficult. Our data are suggestive of a bimodal DAV distribution in temperature. We hope to investigate this issue further by observing additional DAV candidates in the range 11350–11500 K with our collaborators.

2.2. Non-Uniform Detection Efficiency

The hDAVs show relatively few pulsation modes, with low amplitudes ($\sim$0.1–3%) and periods around 100–300 s. The cooler DAVs (cDAVs) typically show longer periods, around 600–1000 s, larger amplitudes (up to 30%), and greater amplitude variability (Kleinman et al. 1998). Massive pulsators show low amplitudes as a result of their high gravity (log $g \geq$ 8.6). These distinct trends of the pulsation periods and amplitudes with temperature and log g imply that the detection efficiency must also be a function of T_{eff} and log g. The detection efficiency not only varies in the T_{eff}–log g plane, but is also dependent upon weather conditions and the magnitude of the DAV candidate. Furthermore, a ZZ Ceti star may have closely spaced modes or multiplet structure, both of which cause beating effects. Some of the non-variables in the instability strip could well be pulsators, that were in the low amplitude phase of their beating cycle during the observing run. McGraw (1977) claimed BPM 37093 to be non-variable, but Kanaan et al. (1992) showed that it is a low amplitude variable with evident beating. Dolez, Vauclair, & Koester (1991) claimed the non-variability limit of G 30-20 to be a few mmag[1], but Mukadam et al. (2002) found G 30-20 to be a beating variable with an amplitude of 13.8 mma[2].

In order to address these issues systematically, we simulate light curves of real pulsators for different conditions and compute the resulting Fourier Transform (FT) to see if the signal is detectable above noise. We utilize the real periods and amplitudes, with randomly chosen phases (to sample the beat period), to simulate two hour long light curves[3]. We independently shuffle the magnitudes and average seeing conditions of real data on the DAVs. This ensures a realistic distribution for both these parameters. We randomly select a magnitude and seeing value from these distributions to simulate white noise, the amplitude of which is determined using a noise table based on real data. We compute a FT of the light curve and check if the star can be identified as a pulsator or if the signal was swamped by noise. We repeat this procedure 100 times for each DAV for different phases, magnitudes,

---

[1]One milli-magnitude (mmag) equals 0.1086% change in intensity.

[2]One milli modulation amplitude (mma) corresponds to 0.1% change in intensity.

[3]We generally observe the DAV candidates for two hours at a time when searching for new variables.

and seeing values. Note that our noise simulation is not completely realistic, as it does not include effects due to variable seeing, gaps in the data due to clouds, and low frequency atmospheric noise. However, it does help us understand how the detection efficiency changes in the T_{eff}–log g plane.

We find that we are able to *rediscover* almost all of the average and low mass cDAVs in the hundred simulated attempts. The high mass (log $g \geq 8.6$) DAVs with a substantially lower amplitude are recovered with a ∼70% success rate. This implies that non-variables in Figure 1 in the region log $g \geq 8.6$ have a 30% chance of being low amplitude variables. At the hot end of the instability strip, both low pulsation amplitude and beating can cause us to miss even the average or low mass hDAVs 35 out of 100 times.

Table 1 lists the non-variables in the instability strip along with their temperature, log g, magnitude, and number of observing runs. The number after the NOV designation indicates the best non-variability limit in mma. Based on the simulations, we assign each non-variable a weight based on our estimate of the probability that the observed candidate is a genuine non-variable, and not a low-amplitude or beating pulsator. We use the non-variability limits to assign the weights 0.98, 0.95, 0.90, 0.85, 0.80, 0.70, and 0.60, for NOV1, NOV2, NOV3, NOV4, NOV5, NOV6, and NOV7 or higher, respectively. If the NOV is massive (log $g \geq 8.6$), then we additionally multiply its weight by a factor of 0.7. If the NOV is close to the blue edge of the strip, then we multiply by a factor of 0.65 to account for low amplitude and/or beating pulsators. However if the NOV has been observed multiple times, then it is unlikely to have been missed as a result of beating. In such a case, we multiply its weight only by a factor of 0.8 instead of 0.65, to allow for a possible low amplitude variable. We utilize these weights in section 6 to compute best-fit red and blue edges.

Table 1.   Non-variables in the ZZ Ceti instability strip

Object	Limit	Obs. Runs	SDSS T_{eff} (K)	SDSS log g	g	Weight
WD0037+0031	NOV5	2	10960 ± 050	8.41 ± 0.03	17.5	0.80
WD0050−0023	NOV6	2	11490 ± 090	8.98 ± 0.03	18.8	0.50
WD0222−0100	NOV3	4	12060 ± 120	8.12 ± 0.05	18.0	0.60
WD0303−0808	NOV4	2	11400 ± 110	8.49 ± 0.06	18.8	0.85
WD0345−0036	NOV5	3	11430 ± 150	7.76 ± 0.09	19.0	0.80
WD0747+2503	NOV3	3	11050 ± 110	7.93 ± 0.08	18.4	0.90
WD0853+0005	NOV4	2	11750 ± 110	8.11 ± 0.06	18.2	0.55
WD1031+6122	NOV4	2	11480 ± 180	7.68 ± 0.11	18.7	0.85
WD1136−0136	NOV2	1	11710 ± 070	7.96 ± 0.04	17.8	0.62
WD1337+0104	NOV4	2	11830 ± 210	8.39 ± 0.11	18.6	0.60
WD1338−0023	NOV4	1	11650 ± 090	8.08 ± 0.05	17.1	0.85
WD1342−0159	NOV4	2	11320 ± 160	8.42 ± 0.09	18.8	0.85
WD1345+0328	NOV6	1	11620 ± 140	7.80 ± 0.08	18.6	0.70
WD1432+0146	NOV5	1	11290 ± 070	8.23 ± 0.06	17.5	0.80
WD1443−0006	NOV5	1	11960 ± 150	7.87 ± 0.07	18.7	0.80
WD1503−0052	NOV4	3	11600 ± 130	8.21 ± 0.07	18.4	0.85
WD1658+3638	NOV4	4	11110 ± 120	8.36 ± 0.09	19.2	0.85
WD1726+5331	NOV7	1	11000 ± 110	8.23 ± 0.08	18.8	0.60

2.3. Uncertainties in temperature and $\log g$ determinations

The true external uncertainties in the SDSS T_{eff} determinations are likely to be larger than listed in Paper-I. We expect that the external uncertainties are of the order of $300\,\mathrm{K}$. However, the uncertainty that is relevant in determining the width and purity of the instability strip defined by a homogeneous ensemble is the internal uncertainty.

The low signal-to-noise of the blue end of the SDSS spectra reduces the reliability of the $\log g$ values. The H8 and H9 lines depend mostly on gravity because neighboring atoms predominantly affect higher energy levels (Hummer & Mihalas 1970), and their density depends on $\log g$. The external uncertainties in $\log g$ for our ensemble may be as high as 0.1, twice that of the estimated uncertainty for the Bergeron et al. (2004) sample. We find an average $\log g$ of $\simeq 8.10$ for our sample of 31 objects, while the 36 objects in Bergeron et al. (2004) average at $\simeq 8.11$. G 238-53 is common to both samples; Bergeron et al. (2004) derive $T_{\mathrm{eff}}=11890\,\mathrm{K}$ and $\log g=7.91$, while the SDSS determination places G 238-53 at $T_{\mathrm{eff}} = 11820 \pm 50$ and $\log g = 8.02 \pm 0.02$. The temperature values agree within 1σ uncertainties. Temperature is mainly determined by the continuum and the $H\alpha$, $H\beta$, and $H\gamma$ lines; the low S/N at the blue end of the SDSS spectra has a reduced effect on temperature determinations. The well calibrated continuum, extending from 3800–9200 Å provides an accurate temperature determination.

The gradual change in mean mass as a function of temperature for the SDSS DA white dwarf fits is addressed in Kleinman et al. (2004), and Figure 7 of their paper shows a quantitative measure of this systematic effect. The increase in $\log g$ across the width of the instability strip is only ~ 0.02, and implies that our determinations of cDAV masses are negligibly higher. These systematic effects are small in the range of the ZZ Ceti instability strip, and cannot produce either the narrow width or the impurity of the observed strip.

We conduct a simple Monte Carlo simulation to estimate the internal T_{eff} uncertainties of our ensemble. Using the observed pulsation characteristics, we can separate the DAVs into two classes: hDAVs and cDAVs (see section 2.2). We show the observed distribution of the hDAVs and cDAVs in the lowest panel of Figure 2. These distributions are distinct, except for 3 objects. Based on the empirical picture, we conceive that the underlying DAV distribution may look similar to that shown in the topmost panel of Figure 2. We perform a Monte Carlo simulation, drawing hDAVs and cDAVs randomly from the expected DAV distribution, and using Gaussian uncertainties with $\sigma = 300\,\mathrm{K}$. We show the resulting distribution in the second panel; the large uncertainties cause significant overlap between the cDAVs and hDAVs, swamping the central gap. We perform a similar simulation with $\sigma = 200\,\mathrm{K}$ (third panel), and it compares well with the observed distribution considering the small numbers of the empirical distribution. This suggests that the internal uncertainties in

effective temperature for our ensemble are $\sigma \leq 200\,\text{K}$ per object, provided we believe that the hDAVs and cDAVs each span a range of at least $300\,\text{K}$. Note that the internal uncertainties for a few individual objects maybe as large as 250–300 K.

3.   Probing the non-uniform DAV distribution using pulsation periods

The mean or dominant period of a pulsator is an indicator of its effective temperature (see section 2.2). This asteroseismological relation is not highly sensitive, but it provides a technique independent of spectroscopy to study the DAV temperature distribution. We show the distribution of the dominant periods of the SDSS DAVs in Figure 3. The top right panel in Figure 3 shows the number of DAVs per period interval and is suggestive of a bimodal distribution; this increases the likelihood that the dearth of DAVs near the center of the strip is real[4].

4.   Questioning the impurity of the instability strip

Non-variables in the instability strip imply that all DA white dwarfs do not evolve in the same way. This notion has a severe implication: decoding the inner structure of a DAV will no longer imply that we can use the results towards understanding DA white dwarfs in general. Hence we question our findings, and conduct simulations to verify our results. Although we estimate the internal T_{eff} uncertainties to be at most $200\,\text{K}$ in section 2.3, we will conservatively assume $\sigma = 300\,\text{K}$ for all subsequent calculations.

The SDSS spectra do not show any evidence of a binary companion for all the non-variables within the instability strip. Also, we used D. Koester's model atmospheres to ascertain that the SDSS algorithm had chosen a solution consistent with the photometric colors $(u - g, g - r)$ in every case.

We now conduct a Monte Carlo simulation assuming a pure instability strip enclosed by non-variables, as shown in the top panel of Figure 4. Note that we have not included a $\log g$ dependence in our model, as we expect it to be a smaller effect than what we are about to demonstrate. We choose non-variables from outside the strip and add uncertainties chosen randomly from a Gaussian error distribution with $\sigma = 300\,\text{K}$ to determine the NOV

---

[4]We made a similar plot using the dominant periods for the 36 previously known DAVs, but did not find any evidence for a bimodal distribution. Determining the dominant period of the 36 ZZ Ceti stars in the literature proved to be difficult and quite inhomogeneous compared to our own data on the SDSS DAVs.

distribution shown in the middle panel. We find that although non-variables leak into the strip, they are found mostly at the outer edges and their number tails off within the strip. The observed NOV distribution (bottom panel) does not show any signs of tailing off within the instability strip. Rather, it displays the same number of non-variables at the edges as in the center of the strip. This suggests that the instability strip is impure, and that all the NOVs within the instability strip did not leak in due to large T_{eff} uncertainties. We carried out these simulations several times to verify these results.

We compute the likelihood that the instability strip is pure based on the following two criteria. There are two ways in which a non-variable can disappear from the instability strip: subsequent observations show it is a (low amplitude) variable or the internal uncertainties in T_{eff} prove to be large enough to allow the possibility that it may have leaked into the strip. Table 1 lists our estimates of the probabilities that the NOVs found within the strip are genuine non-variables. The chance that NOVs may have leaked into the strip due to large internal uncertainties $\sigma = 300\,\mathrm{K}$ are: 0.35 for WD0037+0031, 0.18 for WD0050-0023, 0.13 for WD0303-0808, 0.04 for WD0345-0036, 0.25 for WD0747+2503, 0.42 for WD0853+0005, 0.15 for WD1031+6122, 0.38 for WD1136-0136, 0.31 for WD1338-0023, 0.11 for WD1342-0159, 0.28 for WD1345+0328, 0.13 for WD1432+0146, 0.25 for WD1503-0052, 0.20 for WD1658+3638, and 0.31 for WD1726+5331. The probability that each of the above non-variables disappear from the instability strip is then: 0.48, 0.59, 0.26, 0.23, 0.33, 0.68, 0.28, 0.62, 0.41, 0.24, 0.50, 0.30, 0.36, 0.32, and 0.59 respectively.

Three or four of the above non-variables may have an inclination angle that reduces the observed amplitude below the detection threshold. Instead of calculating various permutations, we will evaluate the likelihood of the worst case scenario. Let four NOVs that have the least chance of disappearing from the instability strip be the ones that have an unsuitable inclination angle for observing pulsations. In that case, the chance that the instability strip is pure is 0.004%. The impurity of the instability strip suggests that parameters other than just the effective temperature and $\log g$ play a crucial role in deciding the fate of a DA white dwarf, i.e., whether it will pulsate or not.

5. Narrow Width of the ZZ Ceti strip

Computing the width of the instability strip using the effective temperatures of the hottest and coolest pulsators gives us a value, independent of our conception of the shape of the ZZ Ceti strip. Determining whether the blue and red edges continue to be linear for very high ($\log g \geq 8.5$) or very low ($\log g \leq 7.7$) masses is presently not possible with either our sample or the Bergeron et al. (2004) sample. The width of the instability strip calculated

from the empirical edges at different values of log g involves additional uncertainties from our linear visualization of the edges.

The empirical SDSS DAV instability strip spans from the hottest objects G 238-53 and WD0825+4119, both at $T_{eff} = 11820\pm170$ K, to the coolest object WD1732+5905 at $10860\pm$ 100 K. This span of 960 ± 200 K is considerably smaller than the 1500 K width in the literature (Bergeron et al. 1995; Koester & Allard 2000). The hottest pulsator in the Bergeron et al. (2004) sample is G 226-29 at 12460 K and the coolest pulsators are G 30-20 and BPM 24754 at 11070 K. The extent of the instability strip for the Bergeron et al. (2004) sample is then ~ 1400 K.

The drift rates of the stable ZZ Ceti pulsators give us a means of measuring their cooling rates (e.g. Kepler et al. 2000a, Mukadam et al. 2003). Our present evolutionary cooling rates from such pulsators suggest that given a width of 950 K, a 0.6 $M_\odot$ ZZ Ceti star may spend $\sim 10^8$ yr traversing the instability strip. This agrees with theoretical calculations by Wood (1995) and Bradley, Winget, & Wood (1992). The narrow width constrains our understanding of the evolution of ZZ Ceti stars.

6. Empirical Blue and Red Edges

We draw blue and red edges around the DAV distribution that enclose all of the variables. This is shown in Figure 5 by the solid line for the blue edge and the line with dots and dashes for the red edge. These edges also include non-variables within the instability strip.

We now demonstrate an innovative statistical approach to find the best-fit blue and red edges that maximize the number of variables and minimize the number of non-variables enclosed within the strip. To the best of our knowledge, no standard technique can be used to solve this interesting statistical problem. Our statistical approach has two advantages: we are accounting for the uncertainties in temperature and log g values and we are utilizing most of the variables and non-variables in our determination rather than just a handful close to the edge.

This problem has essentially two independent sources of uncertainties: the uncertainties in temperature and log g that shift the location of a star in the T_{eff}–log g plane and the uncertainty concerning the genuine nature of a non-variable. Pulsators masquerading as non-variables can significantly alter our determination of the blue and red edges. Hence, we assign different weights to DAVs and NOVs. Since the DAVs are confirmed variables, we assign them a unit weight. We use the non-variability limit to decide the weight of all the NOVs that lie outside the empirical ZZ Ceti strip, as in section 2.2, while we assign the

weights listed in Table 1 for NOVs within the instability strip.

6.1. Technique

We construct a grid in T_{eff} and log g space in the respective ranges 9000–14000 K and 6.0–10.5 with resolutions of 50 K and 0.05. For each point in the grid, we consider possible blue and red edges that vary in inclination angle relative to the temperature axis from 15 degrees to 165 degrees by half a degree with each successive iteration.

For each point of the grid, and for each possible blue edge, we compute a net count as follows: DAVs on the cooler side of the edge count as +1 each and on the hotter side count as −1 each. NOVs on the hotter side of the edge count as +w, and on the cooler side as −w each, where w is the weight of the corresponding NOV. To determine the best blue edge, we consider all DAVs and NOVs that satisfy $T_{\mathrm{eff}} \geq$ 11500 K. This ensures that the NOVs close to and beyond the red edge do not influence the determination of the blue edge. If the DAV or NOV is within 3σ of the edge, then we determine the net chance that it lies on the hot or cool side of the edge, assuming a Gaussian uncertainty distribution. We multiply this chance with the count for that object, before adding it to the total count. An effect of this choice is that the best edge is determined by the global distribution of DAVs and NOVs, rather than the few close to the edge.

Similarly, we determine the best red edge at each point of the grid by counting DAVs on the hotter side of the edge as +1 and NOVs on its cooler side as +w, and vice versa. We consider all DAVs and NOVs within the instability strip and cooler than 11820 K to compute the best red edge. If the DAV or NOV is within 3σ of the red edge, then its contribution is a fraction of the above, depending on the probability that it lies on one side of the edge or the other.

To test our statistical approach, we input the T_{eff} and log g determinations of the previously known DAVs from Bergeron et al. (2004) along with the SDSS NOVs. The resulting red and blue edges are fairly similar to those of Bergeron et al. (2004), and we attribute most of the difference to using an independent set of NOVs[5]. Figure 5 shows our best-fit for the red edge and our constraint on the blue edge using our statistical approach.
For the blue edge, we determine:
Best-fit log g=4.33 T_{eff} -434.77

---

[5]We cannot use the same set of non-variables as Bergeron et al. (2004) as they did not publish the non-variable parameters or identifications.

$+1\sigma$ log g=1.57 T$_{\text{eff}}$ -106.39
-1σ log g=3.73 T$_{\text{eff}}$ -363.45

For the red edge, we determine:
Best-fit log g=1.036 T$_{\text{eff}}$ -30.12
1σ log g=1.192 T$_{\text{eff}}$ -47.26

6.2. Estimating the Uncertainties

The dominant effect that dictates the uncertainties in the slope (log g dependence) and location (in temperature) of the edges arises as a result of the unreliable nature of the NOVs. Are they genuine NOVs or low amplitude pulsators? Our simulations in section 2.2 show that we miss 30% of high mass pulsators due to their low amplitude. We estimate this should introduce an uncertainty of order 0.2 in the total count for both the red and blue edges. The NOVs close to the blue edge, but within the instability strip, can introduce additional uncertainties in our determination. We add these independent sources of uncertainty in quadrature to obtain an estimated 1σ uncertainty of 0.6 for the red edge and 0.4 for the blue edge. We show these as dotted lines in Figure 5. Our estimates of the 1σ uncertainties clearly show that the red edge is well constrained, and the slope of the blue edge is not.

Note that we already account for the uncertainties in T$_{\text{eff}}$ and log g in determining the red and blue edges. The unreliability of these uncertainties contributes towards an uncertainty in the slope of the edges; this turns out to be a negligible second order effect.

6.3. Comparison with Empirical Edges

We show the empirical blue and red edges from Bergeron et al. (2004) in Figure 5 for comparison. The slopes of the red edges from both samples agree within the uncertainties. But our constraint on the blue edge differs significantly from that of Bergeron et al. (2004), and suggests that the dependence on mass is less severe.

The mean temperature of our sample is 11400 K, while the mean temperature for the Bergeron et al. (2004) sample is 11630 K. The observed extent of our instability strip defined by 31 objects spans 10850–11800 K, while that of Bergeron et al. (2004) spans 11070–

$12460\,\mathrm{K}$[6]. We can consider these values to imply a relative shift of $\sim\!200\,\mathrm{K}$ between our sample and that of Bergeron et al. (2004).

We would also like to point out that our sample is magnitude limited and reaches out to $g = 19.3$. We are effectively sampling a different population of stars, more distant by a factor of 10, than the Bergeron et al. (2004) sample.

6.4. Comparison with Theoretical Edges

In Figure 5, we show the theoretical blue edge from Brassard & Fontaine (1997) due to the traditional radiative driving mechanism; they use a ML2/α =0.6 prescription for convection in their equilibrium models. We also show the blue *and* red edges which we derive from the convective driving theory of Wu & Goldreich (Brickhill 1991; Wu 1998; Wu & Goldreich 1999), assuming ML2/α =0.8 for convection.

We see that the blue edges of the two theories are essentially the same, and would nearly coincide if the mixing-length parameter were tuned. To obtain the red edge of Wu & Goldreich, we have made the following assumptions: (1) the relative flux variation at the base of the convection zone is no larger than 50%, (2) the period of a representative red edge mode is 1000 s, and (3) the detection limit for intensity variations is 1 mma. Within this theory, the convection zone attenuates the flux at its base by a factor of $\sim \omega\tau_C$, where τ_C is the thermal response time of the convection zone, so we have adjusted τ_C such that the surface amplitude $0.5/(\omega\tau_C) \sim 10^{-3}$, equal to the detection threshold.

The observed distribution of variables and non-variables suggests that the mass dependence of the blue edge is less severe than predicted by the models. Both the slope and the location of the red edge we calculate are consistent with the observed variables and non-variables within the uncertainties.

7. Conclusion

Using a statistically significant and truly homogeneous set of 31 ZZ Ceti spectra, we find a narrow instability strip between $10850\,\mathrm{K}$ and $11800\,\mathrm{K}$. We also find non-variables within the strip and compute the likelihood that the instability strip is pure to be $\sim 0.004\%$. Obtaining higher signal-to-noise spectra of all the SDSS and non-SDSS DAVs as well as

---

[6]Excluding G 226-29, the Bergeron et al. (2004) sample spans a width of 1060 K from 11070 K to 12130 K.

non-variables in the ZZ Ceti strip is crucial to improving our determination of the width and edges of the instability strip, and in investigating the purity of the instability strip. This should help constrain our understanding of pulsations in ZZ Ceti stars.

The DAV distribution shows a scarcity of DAVs in the range 11350–11500 K. After exploring various possible causes for such a bimodal, non-uniform distribution, we are still not entirely confident that it is real. The data at hand are suggestive that the non-uniformity of the DAV distribution is real, and stayed hidden from us for decades due to the inhomogeneity of the spectra of the previously known DAVs. However, we are in the domain of small number statistics and unless we investigate additional targets in the middle of the strip, we cannot be confident that the bimodal distribution is not an artifact in our data.

REFERENCES

Bergeron, P., Wesemael, F., Lamontagne, R., Fontaine, G., Saffer, R. A., & Allard, N. F. 1995, ApJ, 449, 258

Bergeron, P., Fontaine, G., Billères, M., Boudreault, S., & Green, E. M. 2004, ApJ, 600, 404

Bradley, P. A., Winget, D. E., & Wood, M. A. 1992, ApJ, 391, L33

Brassard, P. & Fontaine, G. 1997, ASSL Vol. 214: White dwarfs, 451

Brickhill, A. J. 1991, MNRAS, 252, 334

Dolez, N., Vauclair, G., & Koester, D. 1991, NATO ASIC Proc. 336: White Dwarfs, 361

Fontaine, G., Bergeron, P., Lacombe, P., Lamontagne, R., & Talon, A. 1985, AJ, 90, 1094

Fontaine, G., Bergeron, P., Billères, M., & Charpinet, S. 2003, ApJ, 591, 1184

Giovannini, O., Kepler, S. O., Kanaan, A., Wood, A., Claver, C. F., & Koester, D. 1998, Baltic Astronomy, 7, 131

Hansen, B. M. S. et al., 2002, ApJ, 574, L155

Hummer, D. G. & Mihalas, D. 1970, MNRAS, 147, 339

Kanaan, A., Kepler, S. O., Giovannini, O., & Diaz, M. 1992, ApJ, 390, L89

Kepler, S. O., et al. 1991, ApJ, 378, L45

Kepler, S. O., Mukadam, A., Winget, D. E., Nather, R. E., Metcalfe, T. S., Reed, M. D., Kawaler, S. D., & Bradley, P. A. 2000a, ApJ, 534, L185

Kepler, S. O., da Costa, A. F. M., Giovannini, O., & Koester, D. 2000b, Baltic Astronomy, 9, 125

Kleinman, S. J. et al. 1998, ApJ, 495, 424

Kleinman, S. J. et al. 2004, ApJ, in press

Koester, D. & Allard, N. F. 2000, Baltic Astronomy, 9, 119

McGraw, J. T. 1977, Ph.D. Thesis, University of Texas at Austin

Metcalfe, T. S., Montgomery, M. H., & Kanaan, A. 2004, astro-ph/0402046

Montgomery, M. H., & Winget, D. E. 1999, ApJ, 526, 976

Mukadam, A. S., Winget, D. E., & Kepler, S. O. 2001, ASP Conf. Ser. 226: 12th European Workshop on White Dwarfs, 337

Mukadam, A. S., Kepler, S. O., Winget, D. E., & Bergeron, P. 2002, ApJ, 580, 429

Mukadam, A. S. et al. 2003, ApJ, 594, 961

Mukadam, A. S., et al. 2004, ApJ, in press

Robinson, E. L. 1979, IAU Colloq. 53: White Dwarfs and Variable Degenerate Stars, 343

Winget, D. E., Hansen, C. J., Liebert, J., van Horn, H. M., Fontaine, G., Nather, R. E., Kepler, S. O., & Lamb, D. Q. 1987, ApJ, 315, L77

Winget, D. E., Kepler, S. O., Kanaan, A., Montgomery, M. H., & Giovannini, O. 1997, ApJ, 487, L191

Winget, D. E. et al. 2003, ASP Conf. Ser. 294: Scientific Frontiers in Research on Extrasolar Planets, 59

Wood, M. A. 1995, LNP Vol. 443: White Dwarfs, 41

Wu, Y. 1998, Ph.D. Thesis, California Institute of Technology
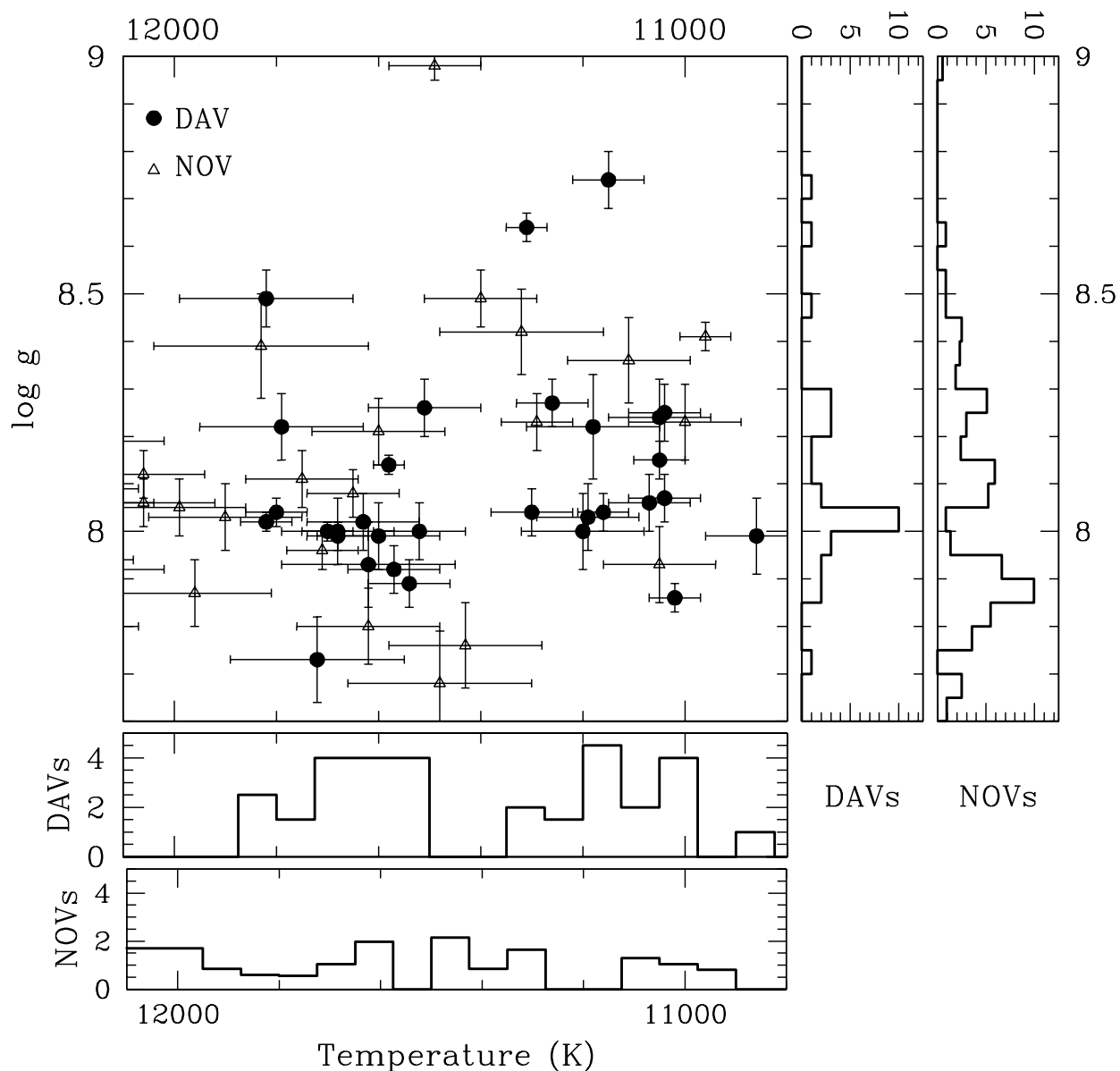
Wu, Y. & Goldreich, P. 1999, ApJ, 519, 783

Fig. 1.— The distribution of new SDSS DAVs and NOVs (Mukadam et al. 2004) as a function of temperature and log g. We also include G 238-53 in this plot. The narrow width of the instability strip and the presence of non-variables within form the two prominent features of this figure. We also note the paucity of DAVs in the middle of the instability strip.
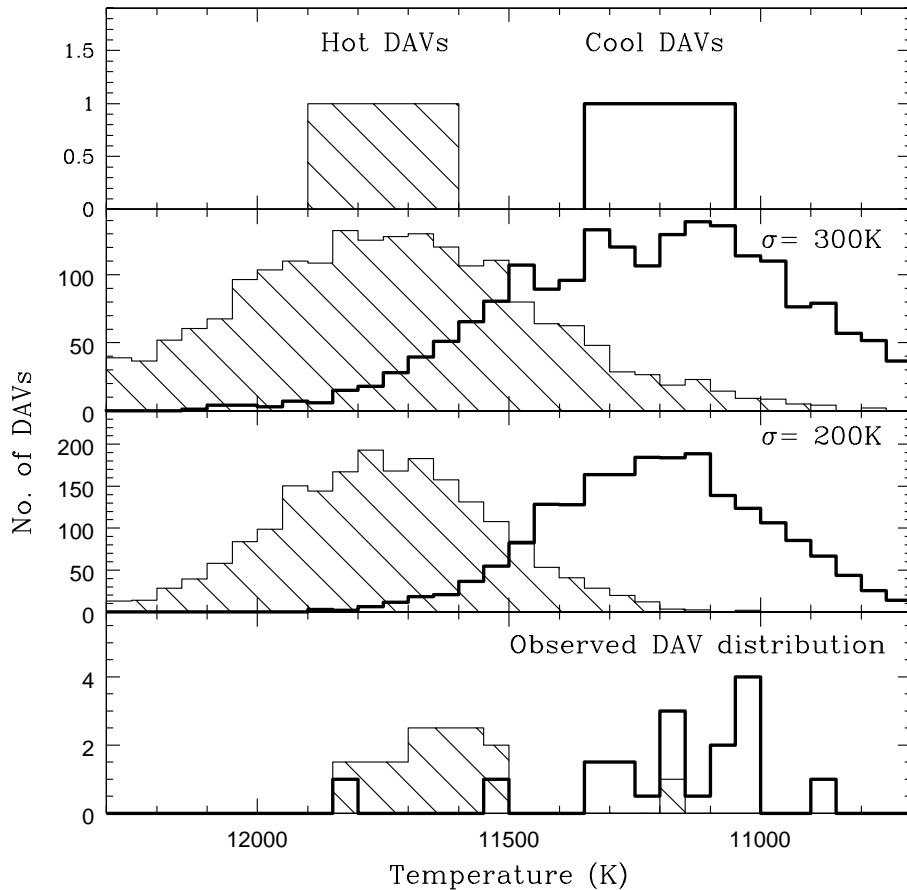
Fig. 2.— We choose hDAVs and cDAVs from the distributions shown in the top panel, and use a Gaussian error function with $\sigma = 300\,\mathrm{K}$ to compute the distributions shown in the second panel. We also similarly determine a DAV distribution with internal uncertainties of order $200\,\mathrm{K}$, shown in the third panel. Comparing the empirical DAV distribution, shown in the bottom panel, to the synthetic computations, we conclude that the average internal uncertainty for our ensemble is $\sigma \leq 200\,\mathrm{K}$.
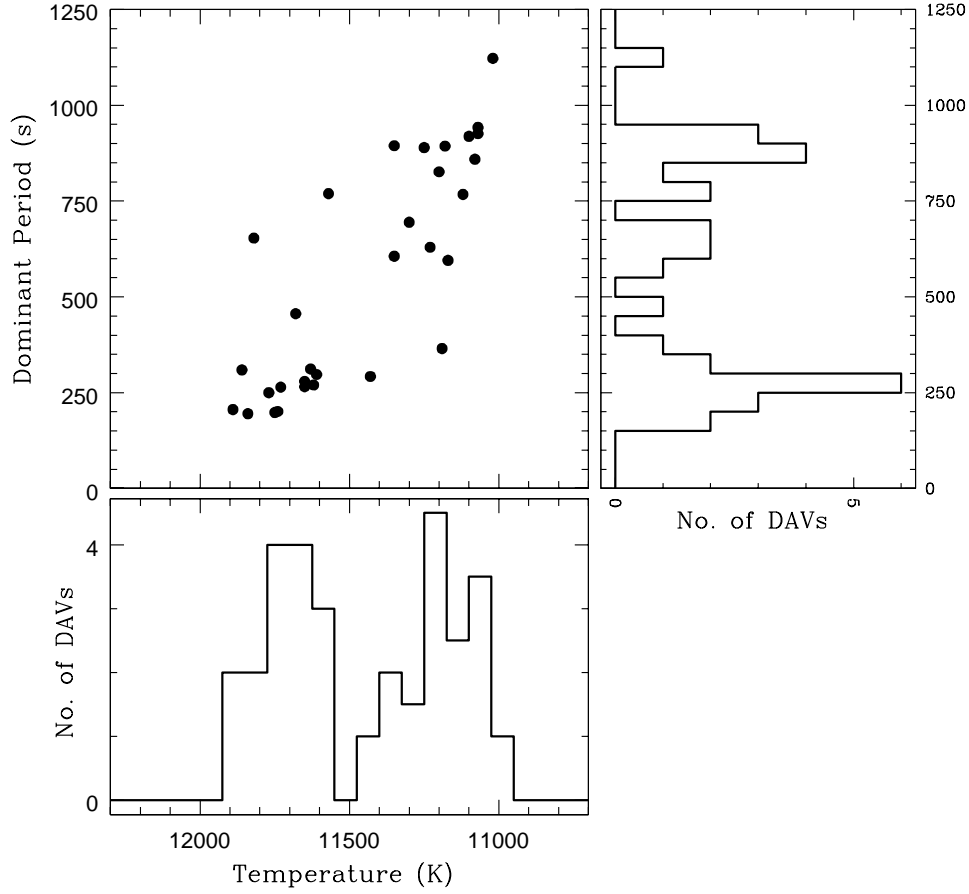
Fig. 3.— Period distribution of the SDSS DAVs as a function of temperature. The top left panel exhibits two distinct clumps consisting of the short period hDAVs and the long period cDAVs. The dominant period of a DAV is a seismological temperature indicator and the histogram shown in the top right panel is suggestive of a bimodal distribution.
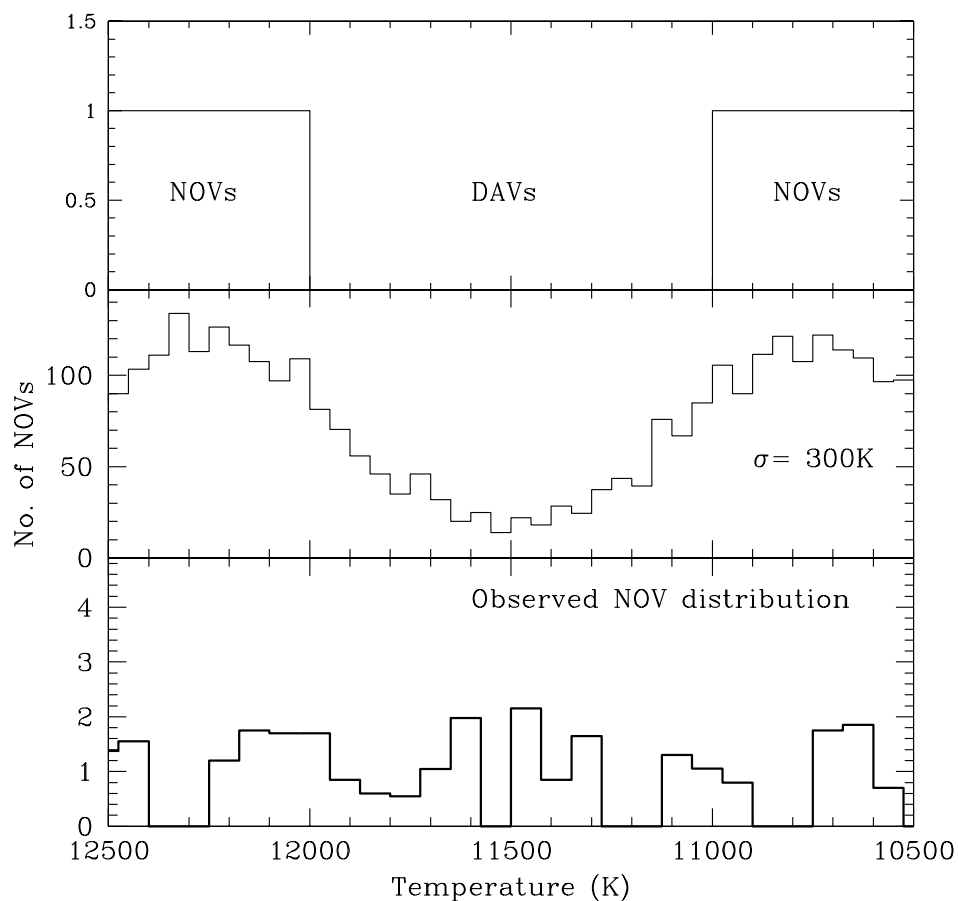
Fig. 4.— Assuming a pure instability strip as shown in the top panel, we use a Monte Carlo simulation assuming a Gaussian distribution for the internal uncertainties with $\sigma = 300$ K to determine the expected distribution for non-variables within the strip. The observed NOV distribution is flat, and shows no signs of tailing off within the strip. The observed distribution shows the same number of non-variables at the edges as in the center of the instability strip.
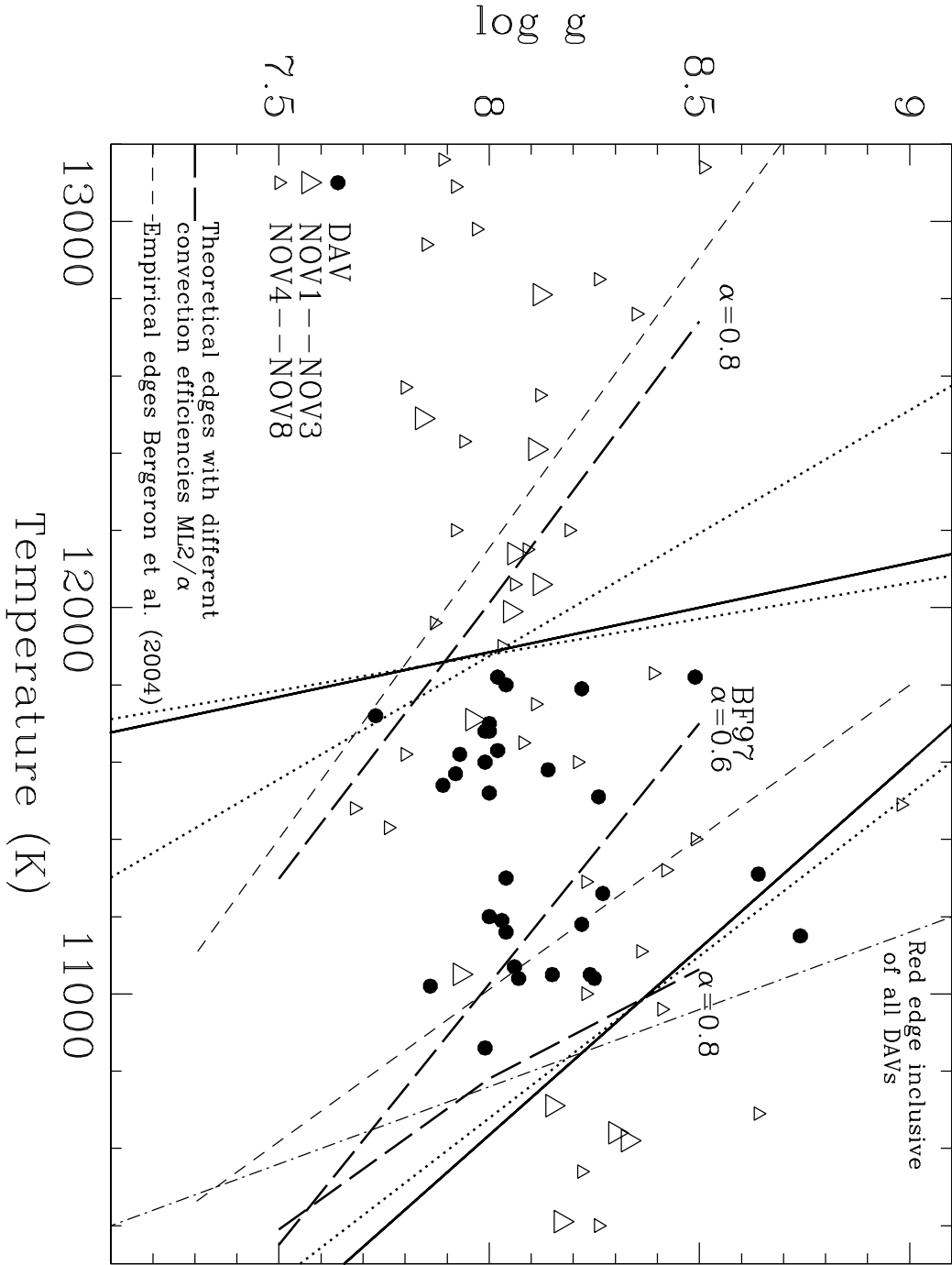
Fig. 5.— Statistical determination of the blue and red edges from the homogeneous set of 31 SDSS DAVs. The thick solid line shows the global solution, while the two dotted lines on either side show the estimated 1σ uncertainty in our determination. Note that the red edge is coincident with one of the dotted lines. Although our blue edge does not exclude any DAVs, our best-fit red edge does. We present the line shown on the extreme right with dots and dashes as a red edge inclusive of all DAVs. We also show the empirical blue and red edges from Bergeron et al. (2004) as dashed lines, and the theoretical blue edge from Brassard & Fontaine (1997; ML2/α=0.6) for comparison. We show our computations of the